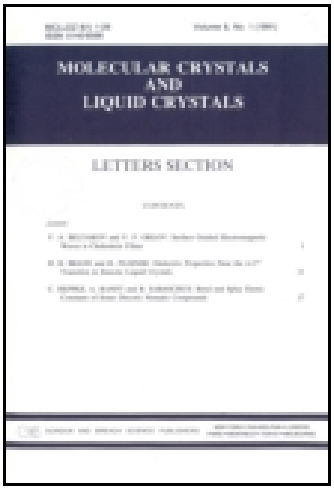


Molecular Crystals and Liquid Crystals
Publication details, including instructions for authors and subscription information:
http://www.tandfonline.com/loi/gmcl20

# Spectroscopy of Charge Transfer Complexes of Aniline Blue

Parimal Trivedi[a], D. N. Bhavsar[a], Sunil Chaki[a], R. G. Patel[a] & A. T. Oza[a]

[a] Department of Physics, Sardar Patel University, Vallabh Vidyanagar, Gujarat, India

Published online: 28 Apr 2014.

To cite this article: Parimal Trivedi, D. N. Bhavsar, Sunil Chaki, R. G. Patel & A. T. Oza (2014) Spectroscopy of Charge Transfer Complexes of Aniline Blue, Molecular Crystals and Liquid Crystals, 592:1, 183-198, DOI: 10.1080/15421406.2013.840058

To link to this article: http://dx.doi.org/10.1080/15421406.2013.840058

*Mol. Cryst. Liq. Cryst.*, Vol. 592: pp. 183–198, 2014

ISSN: 1542-1406 print/1563-5287 online
DOI: 10.1080/15421406.2013.840058

Taylor & Francis
Taylor & Francis Group

# Spectroscopy of Charge Transfer Complexes of Aniline Blue

PARIMAL TRIVEDI, D. N. BHAVSAR, SUNIL CHAKI, R. G. PATEL, AND A. T. OZA*

Department of Physics, Sardar Patel University, Vallabh Vidyanagar, Gujarat, India



*Charge transfer (CT) complexes of aniline blue (AB) were prepared with standard organic acceptors such as TCNQ, TCNE, DDQ, and chloranil and studied with UV-VIS-NIR spectra showing $\sigma \rightarrow \pi^*$ and $\pi \rightarrow \pi^*$ transitions along with free-carrier absorption due to scattering of light particles which has been found involving phonon–photon, electron–photon, and electron–electron scattering. Infrared spectra contain half power beta density due to hopping conduction and an asymmetric band corresponding to $A(k) = A_0 k\ exp(-bk)$ as absorption associated with diffraction of IR light from the crystalline particles.*

**Keywords** Aniline blue; charge transfer complexes; infrared spectroscopy; ultraviolet-visible-near infrared spectroscopy

## 1. Introduction

Aniline blue (AB) is a blue-colored triphenylmethane dye and is more polarizable than green malachite. Although it is stabilized partially with a chloride ion, it forms charge transfer (CT) complexes of still deeper colors with organic acceptors because of its residual molecular free valence. AB itself has very less activation energy.

AB is a triphenylmethane dye [1] having photoconductivity $I_{photo}/I_{dark} = 10^3$, low activation energy of the order of 0.2 eV and is highly reactive as a donor [2,3]. The high reactivity is due to one electron-donating $NH_2$ group, one electron-withdrawing methyl group and two phenyl groups in side chains along with attached NH groups (Fig. 1). On the basis of above criteria, AB was selected in the study of organic semiconductors. Till now only homonuclear organic photoconductors have been studied [3,4]. So, it was our curiosity to understand effect of CT on photo-conducting nature of AB. The subject of photoconductors is well developed [5–7].

There has been renewed and continued interest in organic conductors which is an otherwise old subject [2–4]. Recently CT complex of ethylcarbazole dye and dicyanonapthoquinone were studied using X-ray diffraction method [8]. Electron transfer reaction of 1,2-dimetallocyclohexyl-3,5-dienes with TCNE was studied [9]. PTP-TCNQ where PTP = 2,5-(2-dipyridyl-1,2,4-triazol-3-y(phenol)) was also studied with X-ray diffraction and electrical conductivity measurements [10]. Many $TCNQF_4$ complexes also have been an

*Address correspondence to A. T. Oza, Department of Physics, Sardar Patel University, Vallabh Vidyanagar-388120, Gujarat, India. Tel.: +91989889500. E-mail: ajayozat@yahoo.com

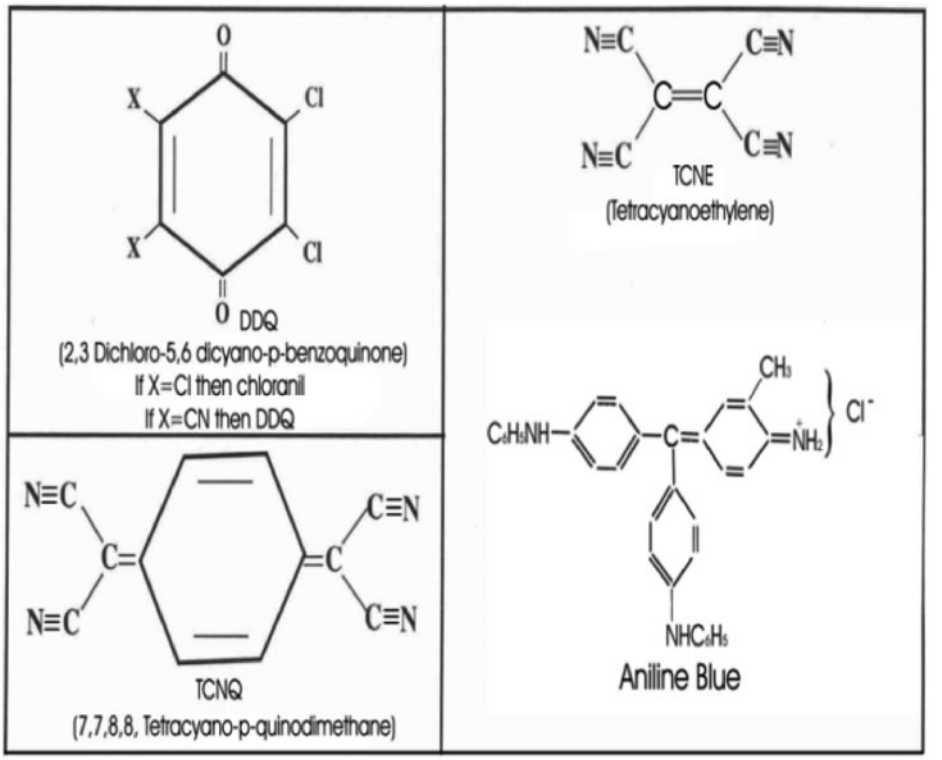


**Figure 1.** Molecular structure of AB and acceptors.

interest of recent study [11]. Perylene-tetracarboxylic dianhydride films were studied with electron diffraction [12]. CPDT-STF-TCNQ was found to be metallic at low temperatures [13]. CT complexes of 1,3-dihexacanyl imidazolium with TCNQ were prepared and structural and electrical resistivity measurements showing activation energy of 0.1 eV were carried out [14]. CT complexes of 2,3-diaminonaphtalyne and chloranil was prepared and studied crystallographically [15]. Several amino acids and related materials were also found to react with chloranil and spectroscopic studies were carried out [16].

In the light of the above interest, we study the effect of CT complex formation on the photoconductivity of organic photoconductors. Triphenylmethane dyes show high photoconductivity with $I_{photo}/I_{dark}$ ratio upto $10^5$–$10^6$. So, we selected AB to form complexes with TCNQ, TCNE, DDQ, and chloranil. The molecular structures of AB and organic acceptors are shown in Fig. 1.

## 2. Experimental Procedure

AB was obtained from Sigma Aldrich Company (St. Louis, MO, USA) as a chloride. Chlorine was not removed while preparing CT complexes with organic acceptors such as TCNQ (7,7,8,8-tetracyano-p-quino-dimethane), TCNE (tetracyano-p-ethylene), DDQ (2,3-dichloro-5,6-dicyano—p-benzoquinone) and chloranil (2,3,5-6-tetrachloro-p-benzoquinone). The preparation of CT complexes involved grinding of AB with organic acceptors in an agate mortar with agate pastle.

The samples for UV-VIS-NIR spectra were in the form of pastes sticking on transparent strips with paraffin oil as a medium have been taken. These samples were placed in a dark chamber of λ model spectrometer of Perkin-Elmer Company and the spectra were recorded in the range of 200 nm to 1600 nm.

AB formed green colored complexes with TCNQ, DDQ, and chloranil and coffee colored complex with TCNE. Semitransparent pallets were prepared by compressing powders in die after mixing with dry spectrograde KBr powder. These pallets were placed in a GXFTIR spectrophotometer for recording the IR spectra in 400–4000 $cm^{-1}$ range. It was a single beam spectrophotometer manufactured by Perkin-Elmer Company of USA. Scan range 15,000—15,030 $cm^{-1}$, scan time 20 scan/sec and OPD velocity of 0.2 cm/sec, and resolution of 0.15 $cm^{-1}$ were adjusted. MIRTGS and FIRTGS were used as detectors Spectra were recorded in purge mode.



## 3. Results and Discussion

First consider the spectrum of AB-TCNQ which is shown in Fig. 2(a). This is a UV-VIS-NIR spectrum. The dip in transmission at 250 nm corresponds to absorption due to $\sigma \rightarrow \pi^*$ transition in TCNQ molecule. Other transmission minimum exists at 380 nm which has broad base like a Lorentzian line shape. It is associated with a $\pi \rightarrow \pi^*$ transition on AB molecule. This band is common in all the four complexes of AB.

Beyond 420 nm, absorption increases as the wavelength of light increases and therefore corresponds to free carrier absorption. When there are free-charge carriers with delocalization, this absorption should be proportional to $\lambda^2$. However, in semiconductor, it is proportional to other powers of λ. When acoustic phonons scatter charge carriers, it is proportional to $\lambda^{1.5}$ when optical phonons scatter charge carriers, it is proportional to $\lambda^{2.5}$ and when ionized impurities scatter the charge carriers, it is proportional $\lambda^{3.5}$ [17–19]. Rayleigh scattering or localized impurity levels leads to $\lambda^4$ dependence. In the case of formation of an impurity band, absorption is proportional to $\lambda^5$ [20]. Free carrier absorption proportional to $\lambda^x$ with $x < 1$ is also found sometime. This is related with the scattering occurring among light (not heavy) particles. In many organic photoconductors and their CTCs, this type of dependence is observed [21]. The exponents of powers can be grouped in three categories. $x = 0.06$ to 0.15, $x = 0.2$ to 0.3, and $x = 0.6$ to 0.8. This can be ascribed to photon-phonon scattering, electron-photon and electron-electron scattering respectively [21]. In photon–phonon scattering, neutral particles are involved and there is no coulomb interaction similar to scattering of electrons by acoustic phonons. In electron–photon scattering, electron-hole pairs are formed and there is dipole moment associated with pairs. This is similar to electron-optical phonon scattering involving ionic dipoles. In electron–electron scattering, coulomb repulsion is involved and the exponent is higher similar to electron impurity scattering.

In AB-TCNQ, log*A* vs. logλ is plotted for analyzing the free carrier absorption. There are two ranges (Figs. 2(b) and (c)) having two slopes 0.09 and 0.11. This corresponds to phonon–phonon scattering. Mainly it involves scattering of photons by acoustic phonons and optical phonons Brillioun and Raman scattering are included.

The UV-VIS-NIR spectrum of AB-DDQ is also shown (Fig. 3(a)). In the range 420–820 nm, a slope of 0.15 is found corresponding to photon–phonon scattering and in the range 820–1180 nm, a slope of 0.625 is found corresponding to electron–electron scattering. Thus in AB-DDQ, coulomb interaction is important leading to electron–electron interaction (Figs. 3(b) and (c)). Other bands are due to $\sigma \rightarrow \pi^*$ and $\pi \rightarrow \pi^*$ transitions.

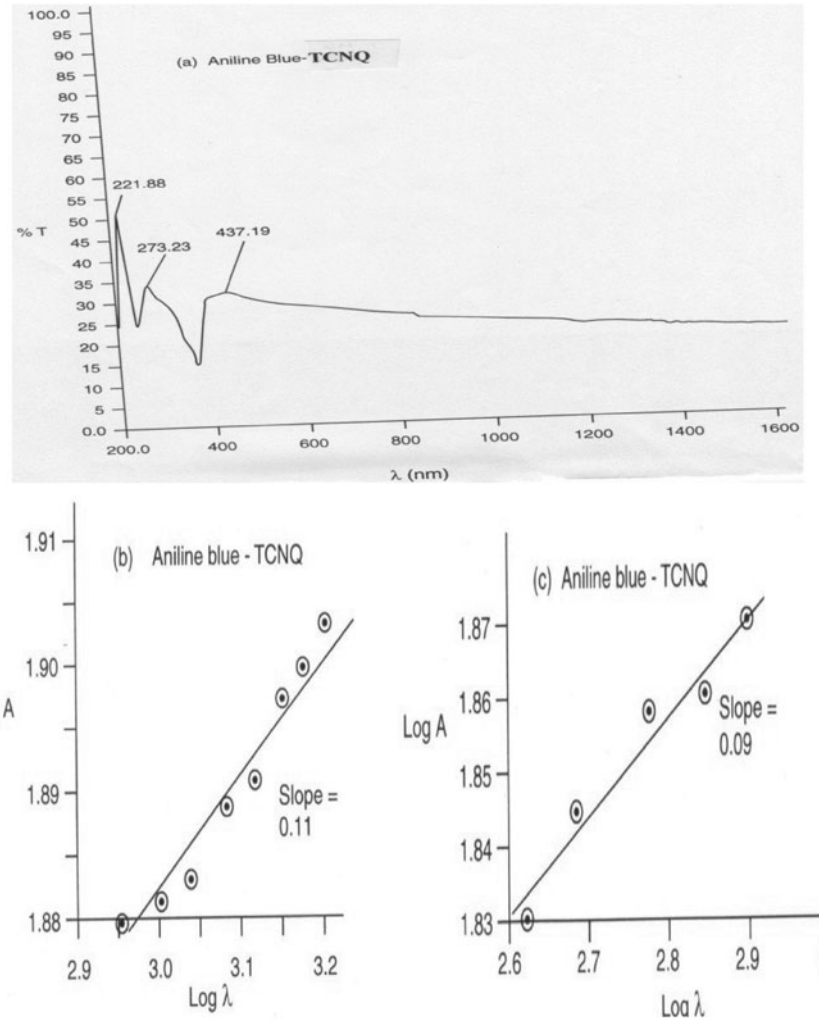


**Figure 2.** (a) UV-VIS-NIR Spectrum of AB-TCNQ. (b) First range of log*A* vs. logλ of AB-TCNQ. (c) second range of log*A* vs. logλ of AB-TCNQ.

The UV-VIS-NIR of AB-TCNE is shown Fig. 4(a). Here also slope of 0.15 associated with photon–phonon scattering is found in the range 430–820 nm and a slope of 0.605 associated with electron–electron scattering is found in the range 1200–1600 nm (Figs. 4(b) and (c)). Bands due to $\sigma \rightarrow \pi^*$ and $\pi \rightarrow \pi^*$ are also observed.

The spectrum of AB-chloranil is also shown in Fig. 5(a). The slope of log*A* vs. logλ is found to be 0.20 revealing electron–photon scattering. In this case, electron-hole pairs are formed and dipoles associated with these pairs interact with photons. AB chloranil is therefore an excitonic semiconductor Fig. 5(b).

The summary of UV-VIS_NIR spectra for all four AB complexes is given in the Table 1.

Next is discussion of the FTIR spectra. FTIR spectra of AB-TCNQ and AB-TCNE are shown in Figs. 6(a) and (b). These spectra contain a broad and intense absorption band between 2800 $cm^{-1}$and 4000 $cm^{-1}$. Above 3600 $cm^{-1}$, there is also a noise spectrum.

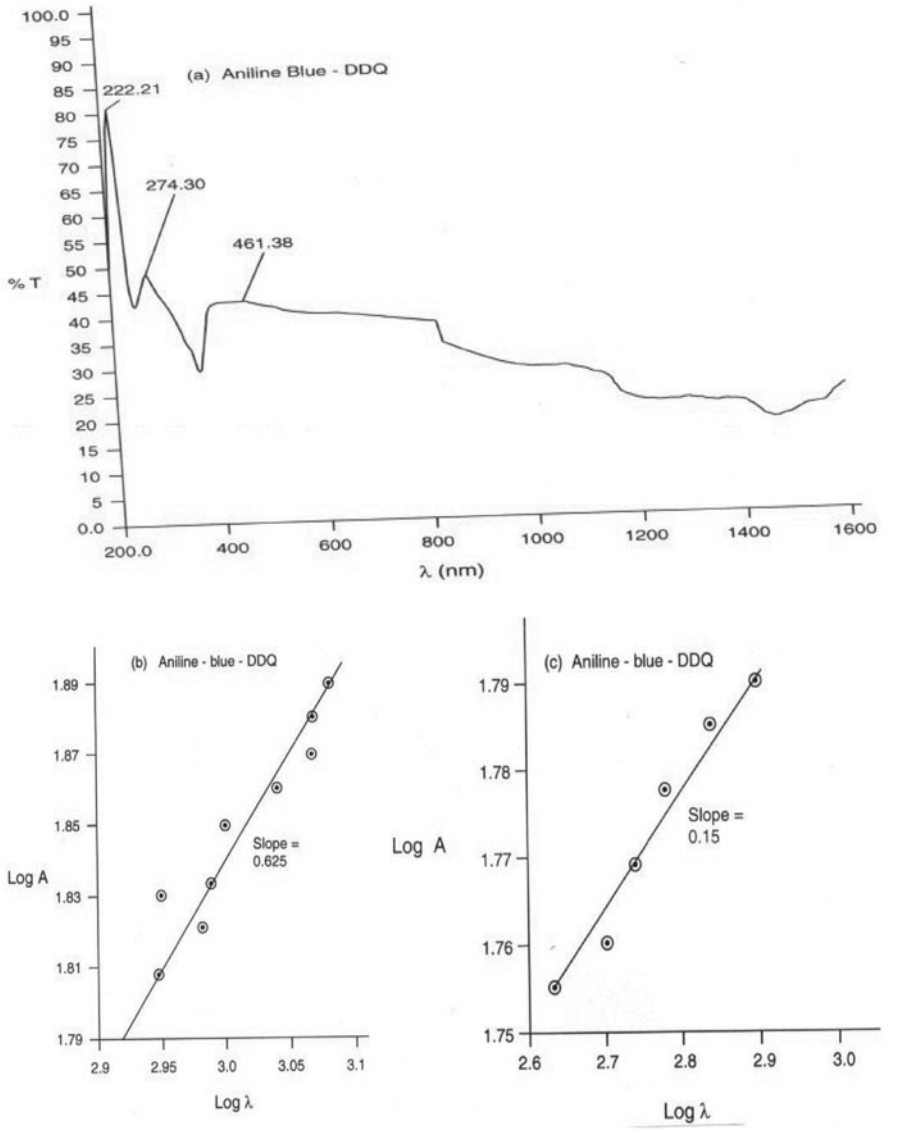


**Figure 3.** (a) UV-VIS-NIR Spectrum of AB-DDQ. (b) First range of log*A* vs. log$\lambda$ of AB-DDQ. (c) Second range of log*A* vs. log$\lambda$ of AB-DDQ.

Between 1800 $cm^{-1}$ and 1000 $cm^{-1}$, there are several stretching and deformation vibrational bands. Between 2800 $cm^{-1}$ and 1800 $cm^{-1}$, there is half power beta density showing a flat peak. Below 900 $cm^{-1}$, there is an asymmetric absorption peak down to 400 $cm^{-1}$ with some fine structure. This transmission dip (absorption peak) follows an absorption function $A(k) = A_0 k \exp(-bk)$. This absorption is fitted by plotting—$\ln(A/k)$ vs. $k$ below 900 $cm^{-1}$ which is shown in Figs. 7(a) and (b).

The slope is positive between 600 $cm^{-1}$ and 800 $cm^{-1}$ and it is negative between 400 $cm^{-1}$ and 600 $cm^{-1}$. There are two interpretations of this asymmetric band. It has a

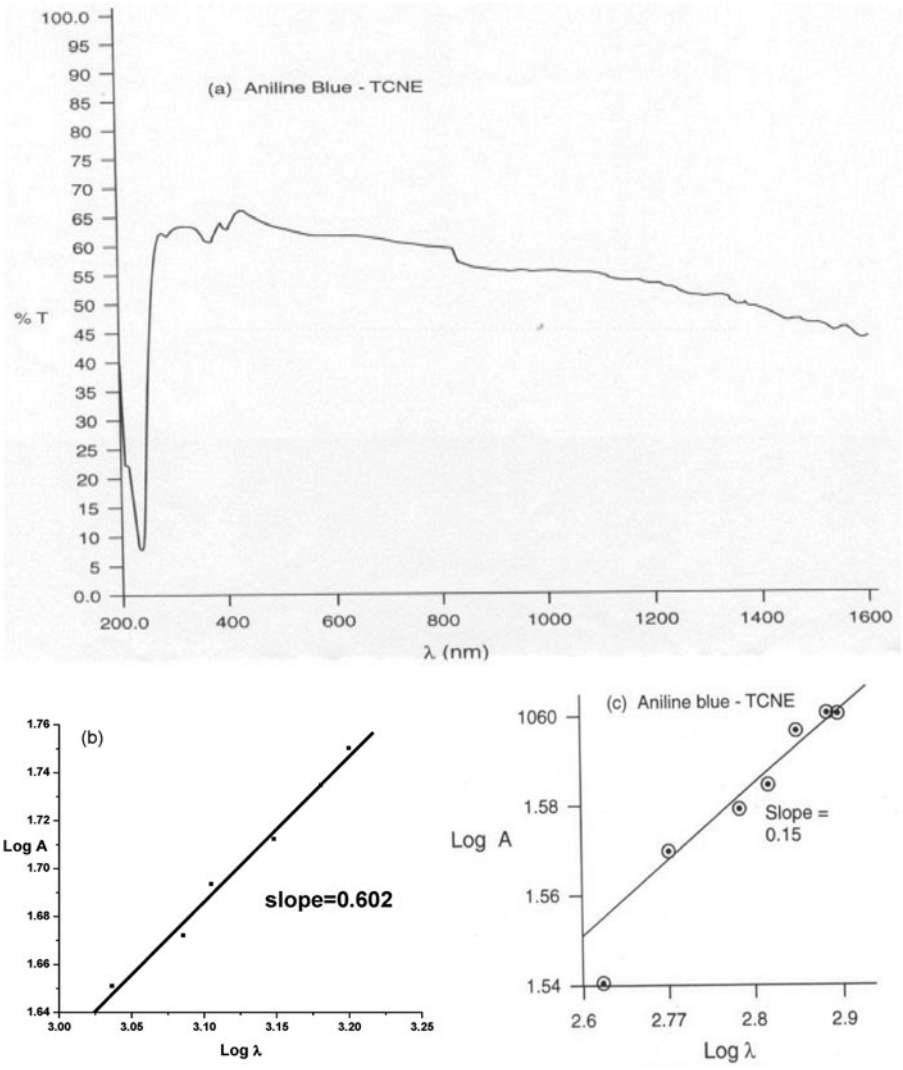


**Figure 4.** (a) UV-VIS-NIR Spectrum of AB-TCNE. (b) First range of log$A$ vs. log$\lambda$ of AB-TCNE. (c) Second range of log$A$ vs. log$\lambda$ of AB-TCNE.

symmetric Fourier transform or a spectral function [22]. This is given by (Eq. 1),

$$A = A_0 \left( \frac{b}{b^2 + \lambda^2} \right) \tag{1}$$

Where $\lambda$ is wavelength, which is the Fourier conjugate of wave vector $k$. The asymmetric peak is due to pinning of charge density waves or phase modulation of charge density waves because one more integration gives (Eq. 2),

$$\int A d\lambda = \frac{A_0}{b} \tan^{-1} \left( \frac{\lambda}{b} \right) \tag{2}$$

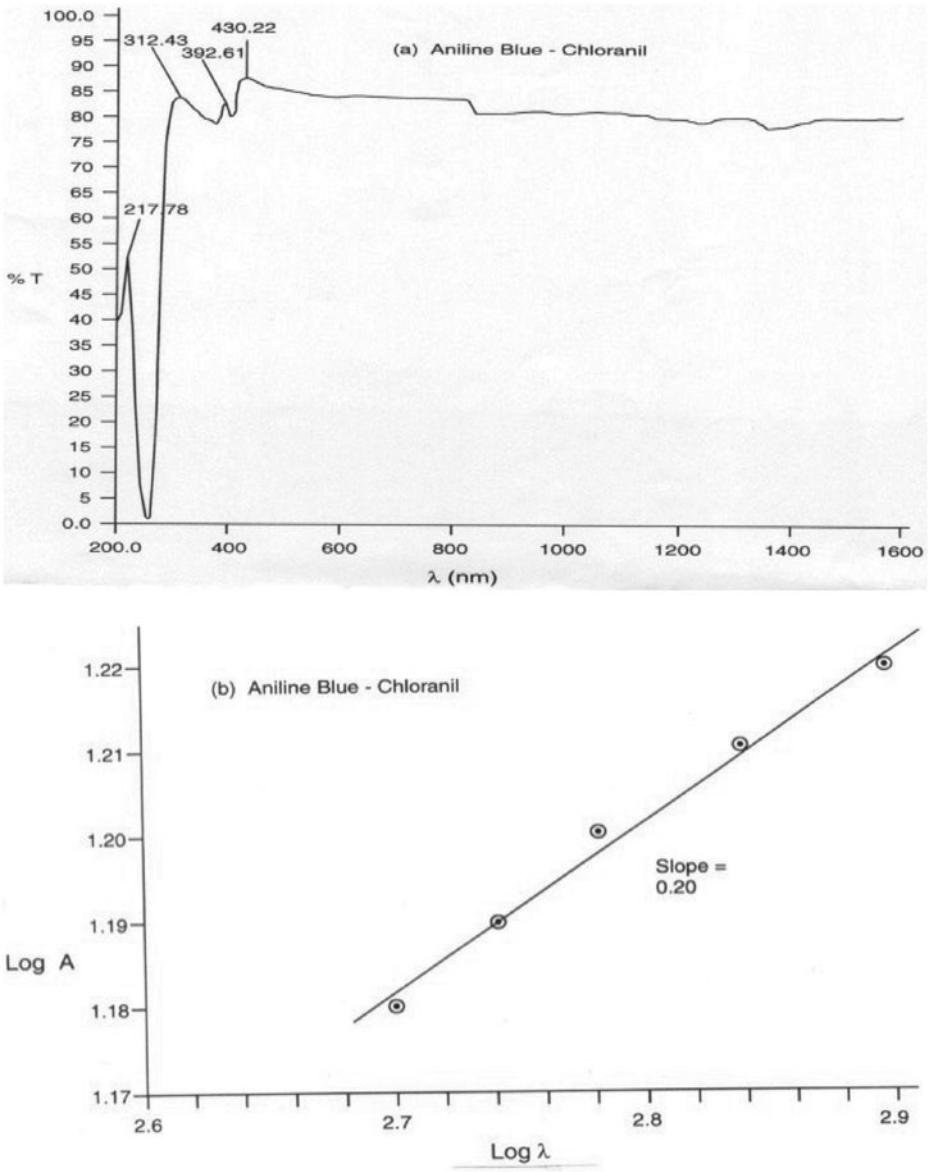


**Figure 5.** (a) UV-VIS-NIR Spectrum of AB-chloranil. (b) log $A$ vs log $\lambda$ in the range of $\lambda = 200$ –820 nm for AB-chloranil.

Where $\tan^{-1}(\lambda/b)$ is the phase angle. Combining above equations (Eq. 3)

$$\int_0^{\infty} A_0 k \exp(-bk) \exp(-ik\lambda) dk d\lambda = \frac{A_0}{b} \tan^{-1}\left(\frac{\lambda}{b}\right) \tag{3}$$

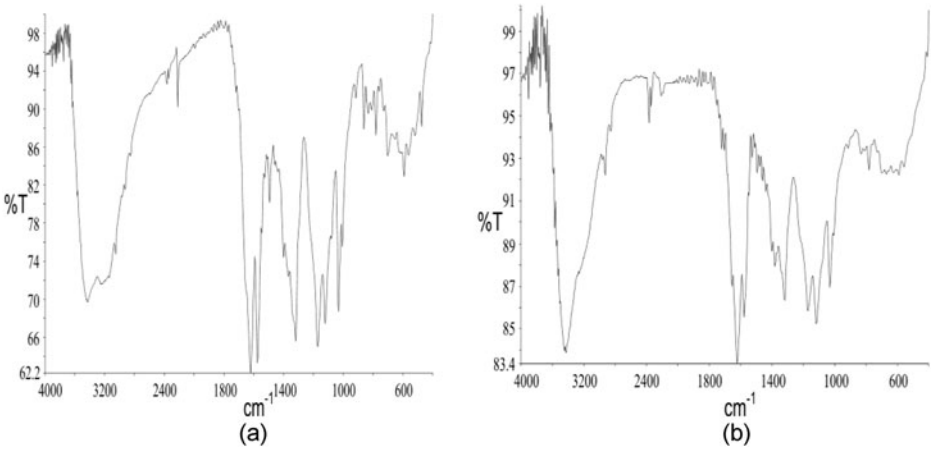


**Figure 6.** (a). FTIR spectra of AB-TCNQ. (b) FTIR spectra of AB-TCNE.

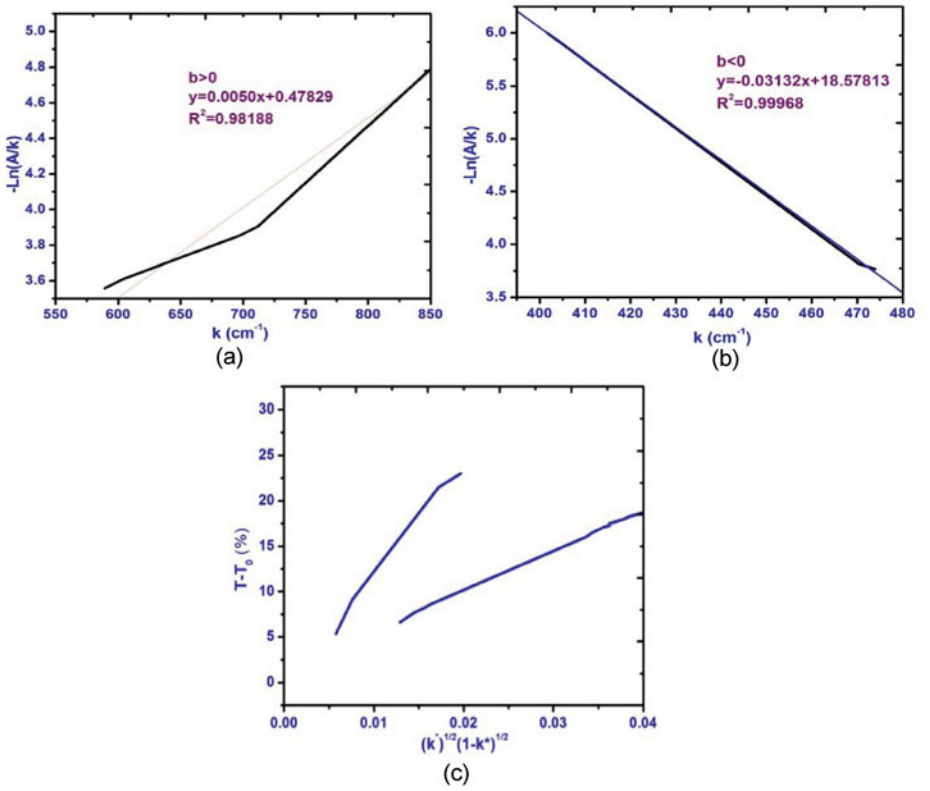


**Figure 7.** (a) Fitting of the absorption function for AB-TCNQ for $b$ greater than zero. (b) Fitting of the absorption function for AB-TCNQ for $b$ less than zero. (c) $T-T_0$ (%) vs. $k^{*1/2}(1 - k^{*})^{1/2}$ for AB-TCNQ.

**Table 1.** Summary of UV-VIS_NIR spectra for all four aniline blue complexes

| | Maximum of wavelength (nm) or range (Slope of Log$A$ vs. Log$\lambda$) | | | |
|---|---|---|---|---|
| Band assignments | AB-TCNQ | AB-TCNE | AB-DDQ | AB-Chloranil |
| $\sigma \rightarrow \pi^*$ | 250 | 240 | 260 | 270 |
| $\pi \rightarrow \pi^*$ | 380 | 400 | 390 | 400 |
| Free carrier absorption (1st range) | 400–820 (0.11) | 430–820 (0.15) | 420–820 (0.15) | 200–820 (0.20) |
| Free carrier absorption (2nd range) | 900–1600 (0.09) | 1200–1600 (0.625) | 820–1180 (0.625) | — |



Then the phase angle $\phi$ satisfies (Eq. 4)

$$\frac{\partial^2 \phi}{\partial \lambda \partial k} = A_0 k \exp(-bk) \exp(-ik\lambda) \tag{4}$$

The second derivative reveals the fluctuation or modulation of the phase angle $\phi$. The asymmetric function $A(k) = A_0 k \exp(-bk)$ arises out of a second order fluctuation in $\phi$ and $\Delta\lambda\Delta k$ is area in phase space.

The parameter $b$ is the distance between neighboring pinning centers. This type of asymmetric band was found in the TTF-TCNQ and TMTSF-DDQ recently and was explained with the above interpretation [23].

There is a second interpretation of asymmetric band which can also arise from the diffraction of infrared light due to size effect of particle size in nano-crystalline material. The distance $b$ turns out to be 36 microns in the range of positive $b$ in AB-TCNQ (Fig. 7(a)) and the infrared light has wavelength below 25 microns having the same order of magnitude. Thus $\lambda \approx b$ leads to diffraction. When $\lambda < b$ there should be reflection, $\lambda \sim b$ there should be diffraction and $\lambda > b$ there should be scattering. Since $\lambda < b$ in AB-TCNQ, there is reflection. This leads to a small range between 400 cm$^{-1}$ and 600 cm$^{-1}$ in which $b$ is negative (Fig. 7(b)). This range is due to the neglection of reflection in calculating $-\ln(A/k)$ where $A = 100 - T$ was taken and not $A = 100 - T - R$ where $R$ is the percentage reflection and $R > 0$ with reduce $A/k$ or $\ln(A/k)$ or increase $-\ln(A/k)$ making $b$ always positive. The angle $\Theta = \tan^{-1}(\lambda/b)$ also becomes negative when $b$ is negative. The negative angle reveals that reflection or backscattering is occurring. The diffraction angle also satisfies (Eq. 5)

$$n\lambda = 2d \sin\theta \tag{5}$$

For $n = 1$ the first order diffraction (Eq. 6),

$$d = \frac{\lambda}{2 \sin\theta} \tag{6}$$

$\lambda$ and $\Theta$ vary but $d$ remains almost constant. The $b$ and $d$ are of the same magnitude. We have also calculated the values of $d$. The transmission between 2800 cm$^{-1}$ and 1800 cm$^{-1}$ satisfies the half power beta density given by (Eq. 7),

$$T = T_0 + Ak^{*\frac{1}{2}} \left(1 - k^* \frac{1}{2}\right) \tag{7}$$

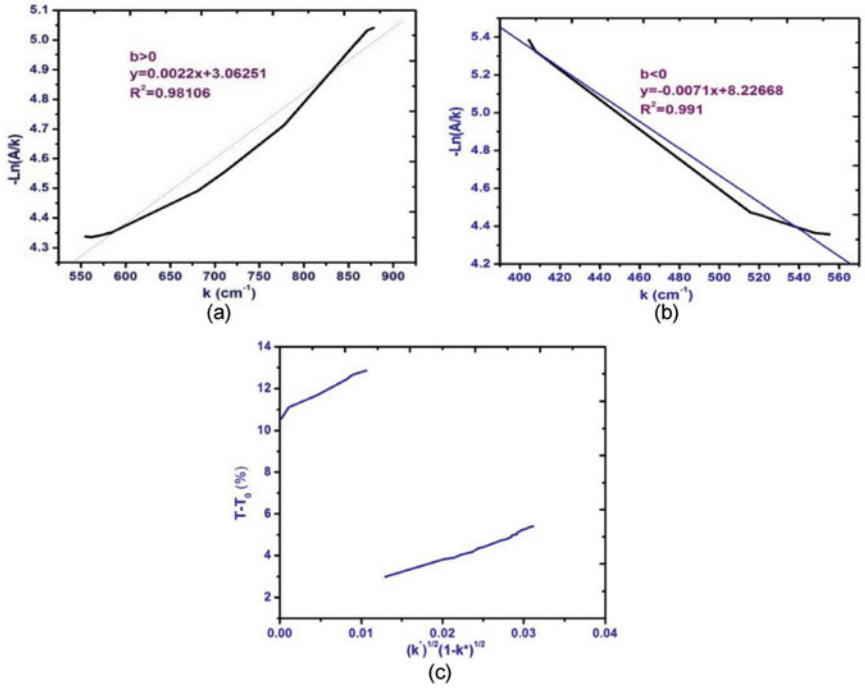


**Figure 8.** (a) Fitting of the absorption function for AB-TCNE for $b$ greater than zero. (b) Fitting of the absorption function for AB-TCNE $b$ less than zero. (c) $T - T_0$ (%) vs. $k^{*1/2}(1 - k^*)^{1/2}$ for AB-TCNE.

By plotting $T - T_0$ (%) vs. $k^{*1/2}\,(1 - k^*)^{1/2}$ this fit is verified which is shown in Fig. 7(c). The beta density based on Bernoulli trials reveals hopping conduction in solids. There is phonon associated hopping in one dimension.

The analysis of $A(k) = A_0 k \exp(-bk)$ and half power beta density for AB-TCNE are also shown in Figs. 8(a–c) respectively. Here, $b$ of 22 microns is found which is of the order of wavelength of IR light. Negative value of $b$ is found below 520 cm$^{-1}$ corresponding to

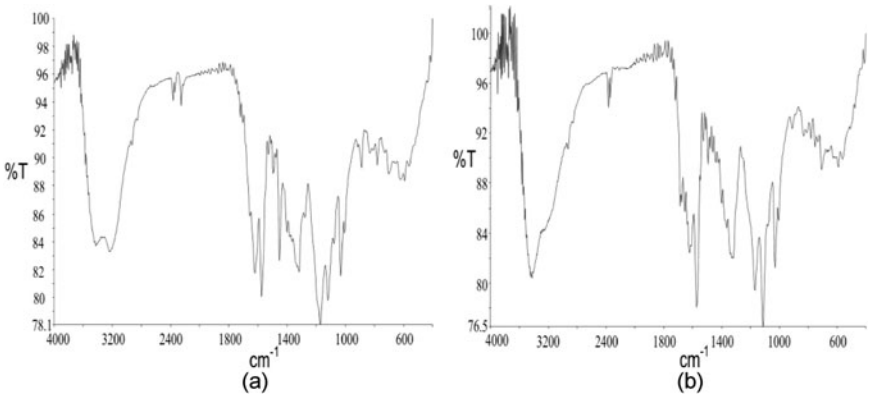


**Figure 9.** (a) FTIR spectra of AB-DDQ. (b) FTIR spectra of AB-Chloranil.

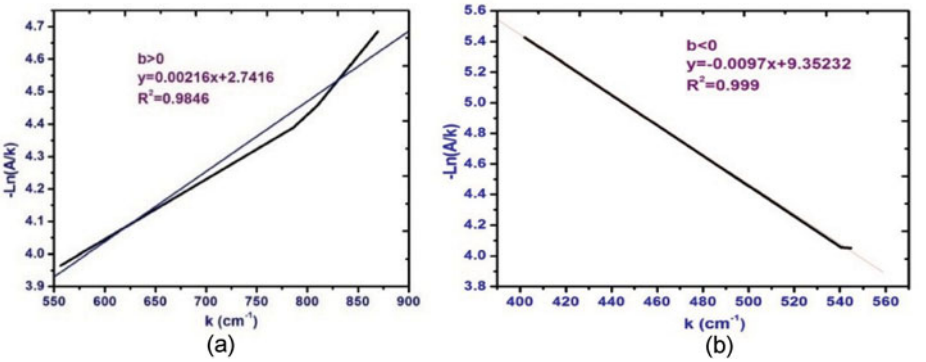


**Figure 10.** (a) Fitting of the absorption function for AB-DDQ for *b* greater than zero. (b) Fitting of the absorption function for AB-DDQ for *b* less than zero.



reflection or backscattering. The half power beta density is found to be asymmetric similar that in AB-TCNQ showing two lines which are not parallel (Fig. 8(c)).

The FTIR spectra of AB-DDQ and AB-chloranil are shown in Figs. 9(a) and (b). These spectra are also similar to those of AB-TCNQ and AB-TCNE complexes. The spectra are governed by donor, that is, AB, molecule. Half power beta density associated with hopping conduction is also visible in these spectra.

The asymmetric background absorption described by $A(k) = A_0 k \exp(-bk)$ is also observed below 850 $cm^{-1}$ (Figs. 10(a—and b) and 11(a and b)). Beta densities are also fitted (Figs. 12(a—and b)).

The value of *b* is 21 micron in AB-DDQ and is 31 micron in AB- chloranil. The negative values of *b* are found below 540 $cm^{-1}$. Thus, all of AB complexes show diffraction of IR light due to the size effect of nanocrystalline or polycrystalline particles.

The band assignments in UV-VIS-NIR spectra summarized in all four complexes of AB (Tables 2 and 3).

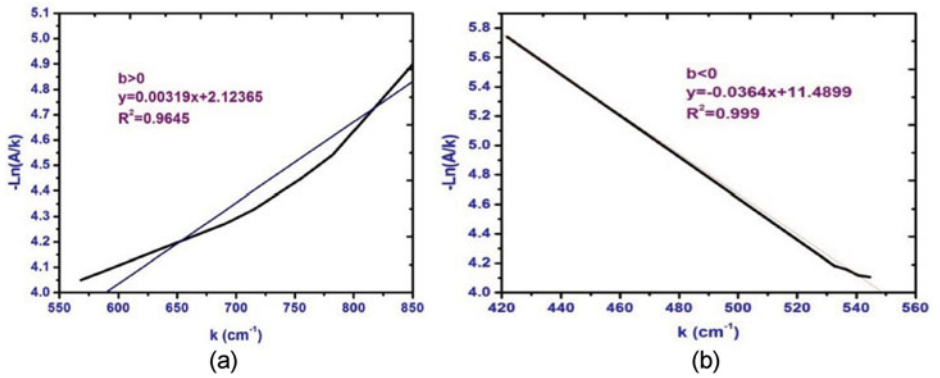


**Figure 11.** (a) Fitting of the absorption function for AB-Chloranil for *b* greater than zero. (b) Fitting of the absorption function for AB-Chloranil for *b* less than zero.

**Table 2.** Band assignments for AB-TCNE and AB-TCNQ

| AB-TCNQ | | AB-TCNE | |
|---|---|---|---|
| Wavenumber ($cm^{-1}$) | Band assignment | Wavenumber ($cm^{-1}$) | Band assignment |
| 3426 (s) | $\nu_{N-H}$ | 3428 (s) | $\nu_{N-H}$ |
| 2222 (w) | $\nu_{C-H}$ | 2929 (m) | $\nu_{C-H}$ |
| 1621 (s) | $\delta_{N-H}$ | 2368 (w) | $\nu_{C-N}$ |
| 1576 (s) | $\nu_{C=N}$ | 2213 (w) | $\nu_{C\equiv N}$ |
| 1494 (m) | $\delta_{C-H}$ | 1622 (s) | $\delta_{N-H}$ |
| 1319 (s) | $\delta_{N-H}$ | 1578 (s) | $\nu_{C=N}$ |
| 1175 (s) | $\nu_{C-C}$ | 1493 (m) | $\delta_{C-H}$ |
| 1120 (s) | $\nu_{C-N}$ | 1381 (m) | $\delta_{N-H}$ |
| 1031 (s) | $\nu_{NH_2}$ | 1319 (s) | $\delta_{N-H}$ |
| 1005 (m) | $\nu_{C-C}$ (ring) | 1166 (s) | $\nu_{C-C}$ |
| 861 (m) | Group vibrations and rocking wagging and twisting of amino group | 1118 (s) | $\nu_{C-N}$ |
| 833 (m) | | 1031 (s) | $\nu_{C-C}$ (ring) |
| 782 (m) | | 780 (m) | Group vibrations of rocking wagging and twisting of amino group |
| 702 (m) | | 592 (m) and many similar bands upto 400 $cm^{-1}$ | |
| 592 (m) | | | |
| 475 (m) | | | |

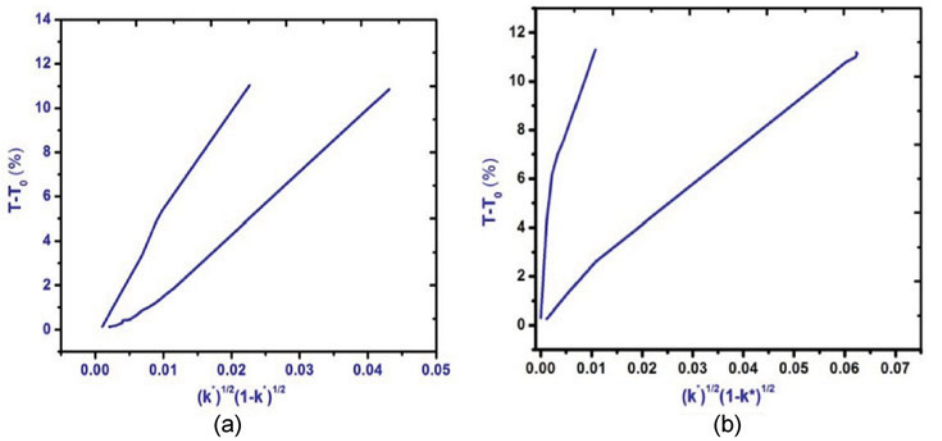


**Figure 12.** (a) $T - T_0(\%)$ vs. $k^{*1/2}(1 - k^{*1/2})$ for AB-DDQ. (b) $T - T_0(\%)$ vs. $k^{*1/2}(1 - k^{*1/2})$ for Chloranil.

**Table 3.** Band assignments for AB-DDQ and AB-Chloranil

| AB-DDQ | | AB-Chloranil | |
|---|---|---|---|
| Wavenumber ($cm^{-1}$) | Band assignment | Wavenumber ($cm^{-1}$) | Band assignment |
| 3423 (s) | $\nu_{N-H}$ | 3426 (s) | $\nu_{N-H}$ |
| 3237 (s) | $\nu_{C-H}$ | 2366 (w) | $\nu_{C-N}$ |
| 2364 (m) | $\nu_{C\equiv N}$ | 1688 (m) | $\nu_{C=C}$ |
| 2253 (m) | $\nu_{C\equiv N}$ | 1623 (s) | $\delta_{N-H}$ |
| 1621 (s) | $\nu_{C=C}$ | 1573 (s) | $\nu_{C=O}$ |
| 1576 (s) | $\nu_{C=O}$ | 1494 (m) | $\delta_{C-H}$ |
| 1453 (s) | $\delta_{C-H}$ | 1320 (s) | $\delta_{N-H}$ |
| 1316 (s) | $\delta_{N-H}$ | 1170 (s) | $\nu_{C-C}$ |
| 1172 (s) | $\nu_{C-C}$ | 1113 (s) | $\nu_{C-N}$ |
| 1119 (s) | $\nu_{C-N}$ | 1031 (s) | $\nu_{NH_2}$ |
| 1031 (s) | $\nu_{NH_2}$ | 1004 (s) | $\nu_{C-C}$ (ring) |
| 888 (s) | Group vibrations of rocking wagging and twisting of amino group | 911 (m) | $\nu_{C-Cl}$ |
| 777 (s) | | 833 (m) | Group vibrations of rocking wagging and twisting of amino group |
| 752 (s) | | 749 (m) | |
| 592 (s) | | 705 (m) | |
| 563 (w) | | 593 (m) | |

The band assignments according to conventional finger-printing method in FTIR spectra of AB complexes are carried out by taking guidance from elsewhere [24–26] and the assignments are tabulated for AB DDQ and AB chloranil in Table 3.

The absorption functions for allowed and forbidden direct as well as allowed and forbidden indirect transitions for both crystalline and amorphous phases were calculated and plotted against photon energy.

**Table 4.** Parameters for Gaussian envelopes

| | High frequency envelope | | | Low frequency envelope | | |
|---|---|---|---|---|---|---|
| Name of the complex | Wave ($cm^{-1}$) | $\alpha_{max}$ (%) | Full width at half maximum $(cm^{-1})^+$ | Wave number ($cm^{-1}$) | $\alpha_{max}$ (%) | Full width at half maximum $(cm^{-1})^+$ |
| AB-TCNQ | 1200 | 36 | 400 (BD) | 600 | 15 | 400 (BD) |
| AB-TCNE | 1200 | 22 | 450 (L) | 850 | 18 | 500 (G) |
| AB-DDQ | 1220 | 22 | 500 (G) | 600 | 10 | 400 (BD) |
| AB-Chloranil | 1120 | 24 | 400 (G) | 675 | 10 | 400 (BD) |

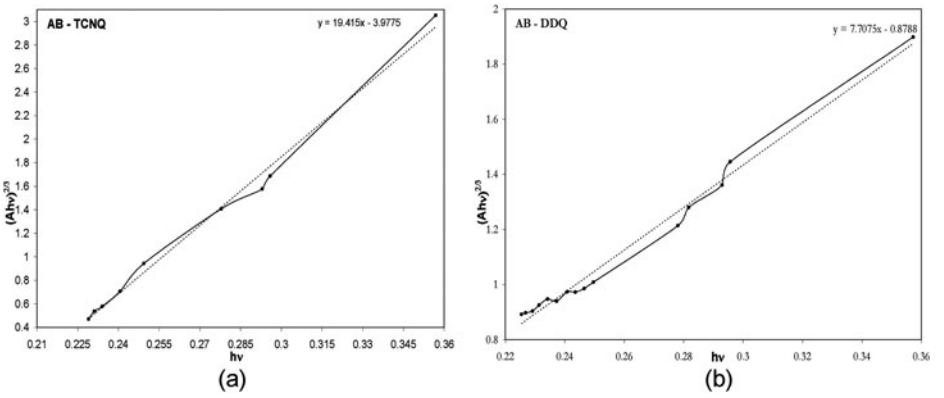


**Figure 13.** (a) Nature of transition in AB-TCNQ. (b) Nature of transition in AB-DDQ.

The best fits for AB-TCNQ and AB-DDQ complexes were found to fit forbidden direct transition described by (Eq. 8) and Fig. 13,

$$\alpha h\nu = A(h\nu - E_g)^{3/2} \tag{8}$$

The Gaussian envelopes observed in high- and low-frequency ranges are having three basic parameters namely wave number maximum, maximum absorption and full width at

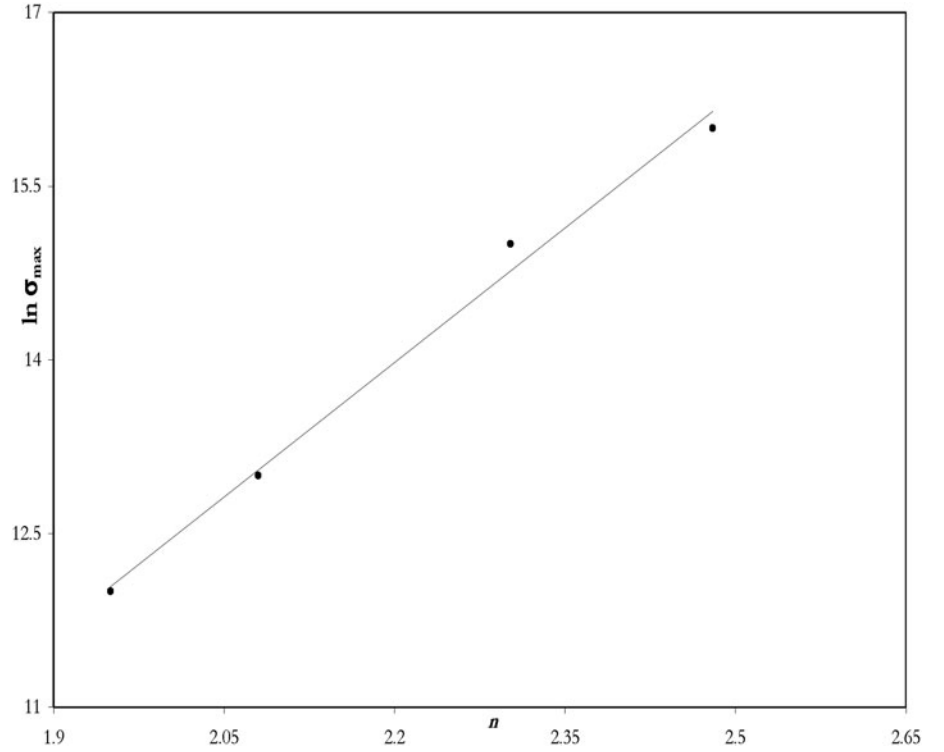


**Figure 14.** Ln $\sigma_{max}$ vs. numbers of bands.

**Table 5.** Values of ln $\sigma$ and number of bands

| Name of the complex | Wave number ($cm^{-1}$) | $\alpha_{max}$ (%) | $\sigma_{max} = \alpha_{max} n_1 c/4\pi$ $sec^{-1}$ | ln $\sigma$ | $n$ |
|---|---|---|---|---|---|
| AB-TCNQ | 1200 | 8 | 10 | 2.302 | 15 |
| AB-TCNE | 1200 | 6 | 7 | 1.95 | 12 |
| AB-DDQ | 1220 | 9 | 12 | 2.48 | 16 |
| AB-Chloranil | 1120 | 7 | 8 | 2.08 | 13 |

half-maximum (FWHM). These parameters are summarized in Table 4. The FWHM is a measure of electron–phonon coupling constant.

Ln $\sigma_{max}$ by calculating $\sigma_{max} = \alpha n_1 c/4\pi$ in $sec^{-1}$ is plotted against $n$ where $n$ is the number of bands coupled in electron-IMV (Intra Molecular Vibration) coupling (Fig. 14).

This correlation is also summarized in Table 5.

## Conclusions

The CT complexes of AB with organic acceptors such as TCNE, TCNQ, DDQ, and chloranil were studied using UV-VIS-NIR and FTIR spectroscopies. The UV-VIS-NIR spectra showed free carrier absorption involving photon–phonon, electron—photon, and electron–electron scattering mechanisms. FTIR spectra showed beta densities associated with hopping mechanism of conduction and asymmetric band corresponding to $A(k) = A_0 k \exp(-bk)$ function related with diffraction of IR light by particles of micron size in polycrystalline samples.

## Acknowledgments

One of the author D. N. Bhavsar is very much thankful to DST INSPIRE Fellowship for providing the necessary financial support to carry out this work as a full time PhD student. We are thankful to the director of SICART laboratory for providing the facility of FTIR Spectra.

## References

[1] Chatwal, G. R. (1988). *Synthetic Dyes, 2nd ed*. Himalaya Publishing House: Bombay-Nagpur-Delhi.
[2] Foster, R. (1969). *Organic Charge Transfer Complexes*, Academic Press: London.
[3] Gutman, F., & Lyons, L. E. (1967). *Organic Semiconductors*, John Wiley: New York.
[4] Kanda, S., & Pohl, H. A. (1968). In: *Organic Semiconducting Polymers*, Katon, J. E. (Eds.), pp. 87–88, Marcel-Dekker: New York.
[5] Gorlich, P. (1961). In: *Advances in Electronics and Electron Physics*, Marton, L. (Ed.), pp. 37–35, Academic Press: New York, 14.
[6] Bube, R. H. (1960). *Photoconductivity of Solids*, John Wiley & Sons Inc.: New York.
[7] Moss, T. S. (1952). *Photoconductivity in the Elements*, Academic Press: New York.
[8] Nakatsu, K., Mochizuki, S., Han, L., Motrnoka, M., & Kitao, T. J. (1991). *J. Dyes Pig.*, *15*, 289.
[9] Mochida, K., Shimizu, H., Kugita, T., & Nanjo, M. (2003). *J. Organomet. Chem.*, *673*, 84.
[10] Bentice, F., Lagrence, M., Montre, O., Wignercourt, J. P., Vezin, H., & Holt, E. M. (2002). *J. Mol. Structure.*, *31*, 51.

[11] Baudron, S. A., Meziere, C., Heuze, K., Fourmigue, M., Batail, P., Molinic, P., & Senziere, P. A. (2002). *J. Solid State Chem.*, *168*, 668.
[12] Shklover, V., Eremtchenko Shostak, Y., Scharfer, J. A., & Sokowskil, M. (2001). *J. Surf. Sci.*, *1241*, 482.
[13] Taniguchi, M., Misaki, Y., Yamabe, T., Tanaka, K., Murata, K., & Mori, T. (1999). *J. Solid State Commun.*, *111*, 559.
[14] Wang, W.-J., Hu, M.-J., Chang, C.-S., Chuang, K.-S., & Chiuand, H.-S., & Sheu, C.-F. (1999). *J. Synt. Metals*., *102*, 1725.
[15] Sung, H. K., Woo, T. L., & Nam Ho, H. (1999). *J. Dyes Pig.*, *41*, 89.
[16] Liu, B. Y., & Cheng, K. L. (1980). *J. Anal. Chim. Acta.*, *120*, 335.
[17] Pankove, J. I. (1971). *Optical Processes in Semiconductors*, Prentice Hall Inc.: Englewood Cliffs, New Jersey.
[18] Fan, H. Y., Spitzer, W. G., & Collins, R. (1956). *J. Phys. Rev. B*, *101*, 566.
[19] Vishvanatahn, S. (1960). *Phys. Rev. B*, *120*, 376.
[20] Kireev, P. S. (1975). *Semiconductor Physics*, Mir Publishers: Moscow.
[21] Trivedi, P. H. (2005). Ph.D. Thesis, Sardar Patel University, Vallabh Vidyanagar, Gujarat, India.
[22] Hsu, H. P. (1970). *Fourier Analysis*, Simon and Schuster: New York, pp. 233–235.
[23] Oza, A. T., Solanki, G. K., Ray, A., & Amin, A. (2010). *Ind. J. Phys.*, *84*, 1527.
[24] Drago, R. (1975). *Physical Methods in Inorganic Chemistry*, East-West Press: New Delhi, pp. 222–223.
[25] Sindhu, P. S. (1985). *Molecular Spectroscopy*, Tata McGraw Hill, pp. 104–105.
[26] Smith, Brian. (1999). *Infrared Spectral Interpretation*, RC Press: Boca Ratan, London-New York-Washington, D.C.